


NANO EXPRESS

Open Access



Increased Curie Temperature Induced by Orbital Ordering in $\text{La}_{0.67}\text{Sr}_{0.33}\text{MnO}_3/\text{BaTiO}_3$ Superlattices

Fei Zhang^{1,2}, Biao Wu^{1,2,3}, Guowei Zhou^{1,2}, Zhi-Yong Quan^{1,2*}  and Xiao-Hong Xu^{1,2}

Abstract

Recent theoretical studies indicated that the Curie temperature of perovskite manganite thin films can be increased by more than an order of magnitude by applying appropriate interfacial strain to control orbital ordering. In this work, we demonstrate that the regular intercalation of BaTiO_3 layers between $\text{La}_{0.67}\text{Sr}_{0.33}\text{MnO}_3$ layers effectively enhances ferromagnetic order and increases the Curie temperature of $\text{La}_{0.67}\text{Sr}_{0.33}\text{MnO}_3/\text{BaTiO}_3$ superlattices. The preferential orbital occupancy of $e_g(x^2-y^2)$ in $\text{La}_{0.67}\text{Sr}_{0.33}\text{MnO}_3$ layers induced by the tensile strain of BaTiO_3 layers is identified by X-ray linear dichroism measurements. Our results reveal that controlling orbital ordering can effectively improve the Curie temperature of $\text{La}_{0.67}\text{Sr}_{0.33}\text{MnO}_3$ films and that in-plane orbital occupancy is beneficial to the double exchange ferromagnetic coupling of thin-film samples. These findings create new opportunities for the design and control of magnetism in artificial structures and pave the way to a variety of novel magnetoelectronic applications that operate far above room temperature.

Keywords: $\text{La}_{0.67}\text{Sr}_{0.33}\text{MnO}_3/\text{BaTiO}_3$ superlattices, High Curie temperature, Orbital ordering, Tensile strain

PACS: 75.47.Lx, 51.60.+a, 68.35.Ct

Background

A common observation in perovskite manganite films is that the Curie temperature (T_C) decreases with the reduction of film thickness, which limits their potential for spintronic devices such as field-effect transistors, magnetic tunnel junctions, spin valves, and nonvolatile magnetic memory [1–5]. This is the so-called “dead layer,” defined as the thinnest layer for which ferromagnetic behavior is observed [6–8]. This dead layer phenomenon may be related to electronic and/or chemical phase separation [9, 10], to growth characteristics and microstructure [11, 12], or to manganese e_g orbital reconstruction [13, 14]. Recently, many efforts have been made to increase the T_C of ultrathin perovskite manganite films by superlattice interface control and precise

strain tuning [15–18]. Among the perovskite manganites, $\text{La}_{0.67}\text{Sr}_{0.33}\text{MnO}_3$ (LSMO) films have drawn increasing interest due to their colossal magnetoresistance effect, high T_C , and half metallicity [19–23]. Also LSMO-based heterostructures have been investigated because of the interfacial couplings and intermixing of atoms etc. [24–28]. M. Ziese et al. reported ferromagnetic order of ultrathin LSMO layers in LSMO/ SrRuO_3 superlattices stabilized down to layer thicknesses of at least two unit cells (u.c.) that exhibits a T_C above room temperature [29]. First principle calculations indicate that the T_C of LSMO films can be increased by more than an order of magnitude by controlling orbital ordering using the regular intercalation of adequate layers in LSMO/ BaTiO_3 (BTO) superlattices. In such a configuration, the LSMO layers with occupied $e_g(x^2-y^2)$ orbitals are associated with a strong in-plane double exchange, resulting in a high T_C [30]. This phenomenon has been observed in temperature-dependent magnetization data [30].

* Correspondence: quanzy@sxnu.edu.cn

¹Key Laboratory of Magnetic Molecules and Magnetic Information Materials of Ministry of Education, School of Chemistry and Materials Science, Shanxi Normal University, Linfen 041004, China

²Research Institute of Materials Science, Shanxi Normal University, Linfen 041004, China

Full list of author information is available at the end of the article

In this work, we synthesized LSMO/BTO superlattices using pulsed laser deposition (PLD) and reveal the relationship between the origin of high T_C and manganese e_g orbital occupancy through the use of X-ray linear dichroism (XLD) measurements. We show that the regular intercalation of BTO layers between LSMO layers can effectively enhance ferromagnetic order and increases the T_C of ultrathin LSMO films due to the orbital occupation of $e_g(x^2-y^2)$ in Mn^{3+} ions. Notably, the origin of the T_C increase is different from the one suggested theoretically by A. Sadoc et al., who showed that only the central LSMO layers contribute to high T_C and that the interfacial layers adjacent to the BTO layers are associated with a weak in-plane double exchange due to $e_g(3z^2-r^2)$ orbital occupation [30]. We find that the preferential orbital occupancy of $e_g(x^2-y^2)$ in both of the central and the interfacial LSMO layers is induced by BTO layer strain, and gives rise to the in-plane double exchange coupling in LSMO/BTO superlattices, resulting in high T_C . Our findings provide a method to design and control magnetism in artificial structures and have potential for spintronic device applications—including spin-valve devices or nonvolatile magnetic memory working at temperatures far above room temperature.

Methods

(001)-oriented $[(\text{LSMO})_3/(\text{BTO})_3]_n$ superlattice (denoted as SL- n , where 3 is the number of unit cells, $n = 3, 4, 10$ is the number of cycles) samples were synthesized on (001) SrTiO_3 substrates using PLD. A stoichiometric polycrystalline target was used in a 100-mTorr oxygen environment at a substrate temperature of 725 and 780 °

C for LSMO and BTO, respectively. A KrF excimer laser ($\lambda = 248$ nm) with a 2 Hz repetition rate was employed. Energy of 350 and 300 mJ was focused on the targets to obtain the LSMO and BTO layers, respectively. After the growth, the samples were annealed in a 300-Torr oxygen atmosphere in situ for 1 h to improve their quality and reduce their inherent oxygen deficit and then cooled to room temperature. As a reference, two LSMO films with 3 and 40 u.c. thickness (denoted as LSMO(3) and LSMO(40), respectively) were also prepared using PLD under the same conditions for comparison with the SL- n superlattices. To grow films epitaxially with atomic precision, we prepared an atomically flat, single-terminated SrTiO_3 surface by etching in an NH_4F -buffered HF solution (BHF) and subsequently annealing in an oxygen atmosphere at a temperature of 960 °C. The surface topography of a BHF-treated, bare (001) SrTiO_3 substrate was characterized by atomic force microscopy (AFM) analysis, as shown in Fig. 1d. The surface is very smooth, and there are clear steps separating the terraces.

The growth process for each film was monitored in situ using real-time reflection high-energy electron diffraction (RHEED) analysis, providing precise control of the thickness at the unit cell scale and an accurate characterization of the growth dynamics. The crystal structures and surface morphologies were investigated using X-ray diffraction (XRD) and transmission electron microscopy (TEM). To confirm the strain in the samples, Raman spectra were also recorded using a microscopic confocal Raman spectrometer (RM2000, Renishaw, England) excited with a 514.5 nm Ar^+ ion laser. The magnetic properties and T_C of the samples

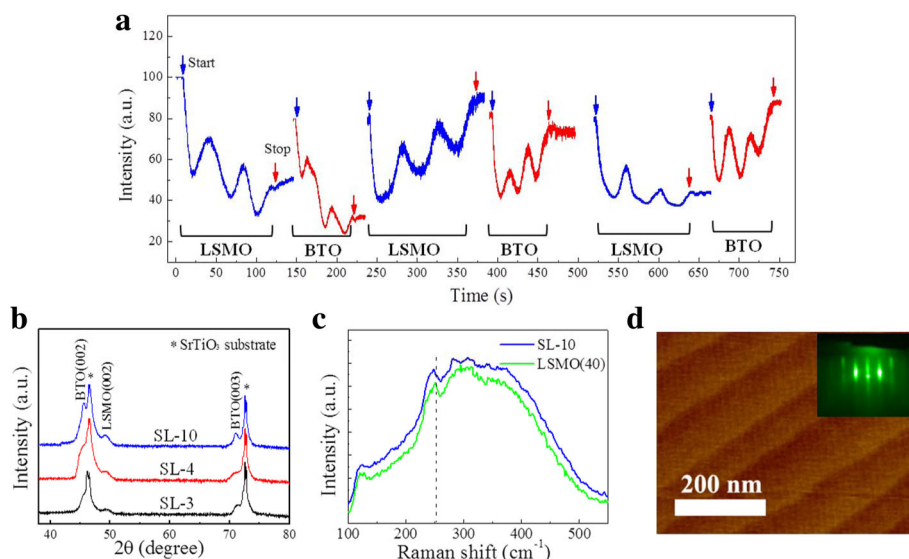
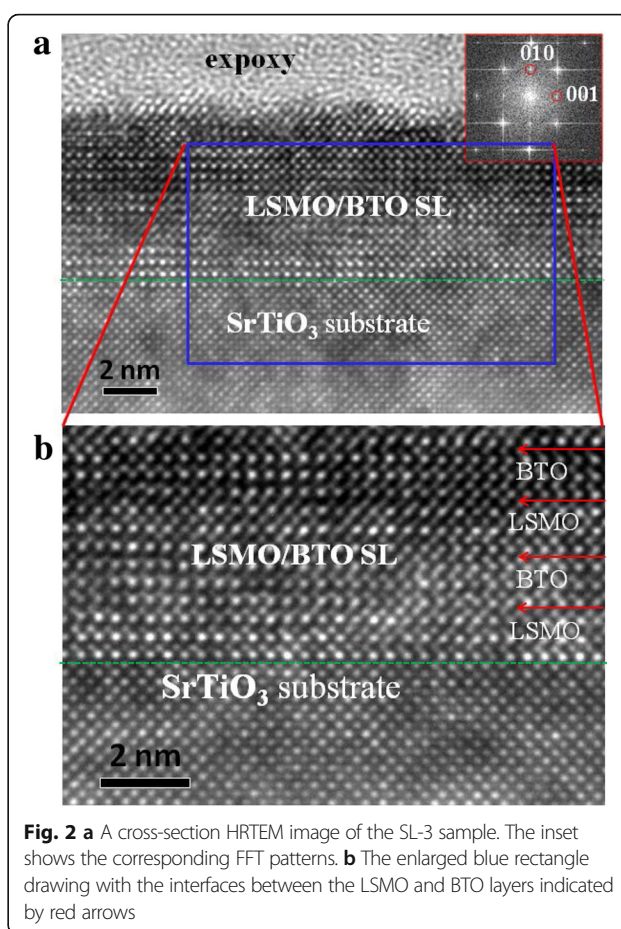


Fig. 1 **a** RHEED intensity oscillations for the growth of the SL-3 sample. **b** XRD patterns for three different SL- n samples ($n = 3, 4, 10$). **c** Raman spectra for the SL-10 and LSMO(40) samples measured at 300 K. **d** AFM image of a BHF-etched, bare (001) SrTiO_3 substrate. The inset shows the RHEED diffraction pattern of the SL-3 sample

were measured with a superconducting quantum interference device (SQUID) magnetometer with in-plane applied magnetic field. The magnetization was calculated after a linear background subtraction of the SrTiO_3 substrate diamagnetic contribution. The transport properties were determined in the Van der Pauw four-point probe configuration using a Quantum Design Physical Properties Measurement System (PPMS) over temperatures ranging from 20 to 365 K. X-ray absorption spectroscopy (XAS) and XLD measurements were made at Beamline BL08U1A of the Shanghai Synchrotron Radiation Facility and U19 of National Synchrotron Radiation Laboratory in the total electron yield (TEY) mode at room temperature.

Results and Discussion

Figure 1a shows the RHEED oscillations recorded during the growth of the SL-3 sample on a TiO_2 -terminated (001) SrTiO_3 substrate. The LSMO and BTO film thicknesses were controlled by counting the RHEED intensity oscillations. For optimized conditions, RHEED oscillations remain visible throughout the superlattice deposition process, indicating a layer-by-layer growth. The inset of Fig. 1d shows the clear streaky RHEED diffraction pattern after the growth of the SL-3 sample. Typical XRD patterns shown in Fig. 1b reveal high-quality growth in the (001) orientation for all three superlattices. As expected, the LSMO peaks shift slightly to a higher angle while the BTO peaks shift to a lower angle (compared to the bulk value), which reflects the strain state of the interfaces between the LSMO layers and the BTO layers (i.e., in-plane cell parameter elongation for LSMO and reduction for BTO). This desired strain can be maintained over the whole film thickness due to the repeating intercalation of LSMO and BTO layers. Raman spectra measured at 300 K for the SL-10 and LSMO(40) samples are shown in Fig. 1c. Compared to LSMO(40) sample, a slight low-frequency shift of bands at 252 cm^{-1} was observed in SL-10 sample, indicating the LSMO layers in SL-10 sample with a tensile strain induced by BTO layers [31–33]. In addition, the high quality of the superlattices was confirmed by TEM. Figure 2a is the cross-sectional high-resolution TEM (HRTEM) of the SL-3 sample on a (001)-oriented SrTiO_3 substrate, endorsing high-quality epitaxial growth of LSMO/BTO superlattice. The inset of Fig. 2a is the corresponding fast Fourier transform (FFT), suggesting that the film is indeed in single phase. Figure 2b shows the enlarged image of Fig. 2a. The image shows atomically sharp interfaces between the LSMO and BTO layers highlighted by red arrows. In the superlattices, there is no obvious interdiffusion at the interfaces, and the LSMO and BTO layers are fully strained to the SrTiO_3 substrates. This observation was consistent with the XRD results.



Next, we present a description of the magnetic properties of the SL- n samples. The temperature-dependent magnetization for SL- n films with $n = 3, 4, 10$, as well as the LSMO(3) sample, are shown in Fig. 3a. Here, the measurement is carried out over a temperature range from 5 to 350 K with a magnetic field (3000 Oe) applied parallel to the surface of the SrTiO_3 substrates. Note that the T_C of the superlattices is significantly improved compared to the LSMO(3) film [6], of which T_C is around 45 K (see the inset in Fig. 3a). For the SL-10 sample, the T_C increases above 265 K compared to the LSMO(3) film and reaches a maximum value of $T_C \sim 310$ K. Figure 3b shows corresponding magnetic hysteresis loops for the four samples measured at 5 K, showing obvious ferromagnetic signal with a saturation magnetization (M_s) of $\sim 1.5\text{ }\mu_B/\text{Mn}$ —except for the LSMO(3) film. Here, the ferromagnetism of the LSMO layers in the SL- n samples comes from the total LSMO triple layers, which is different from those reported by A. Sadoc et al., who showed that the ferromagnetic exchange is just related to the central LSMO layers and is independent of the interfacial LSMO layers adjacent to BTO layers using first principle calculations [30]. Given that ferromagnetism is only derived from the central

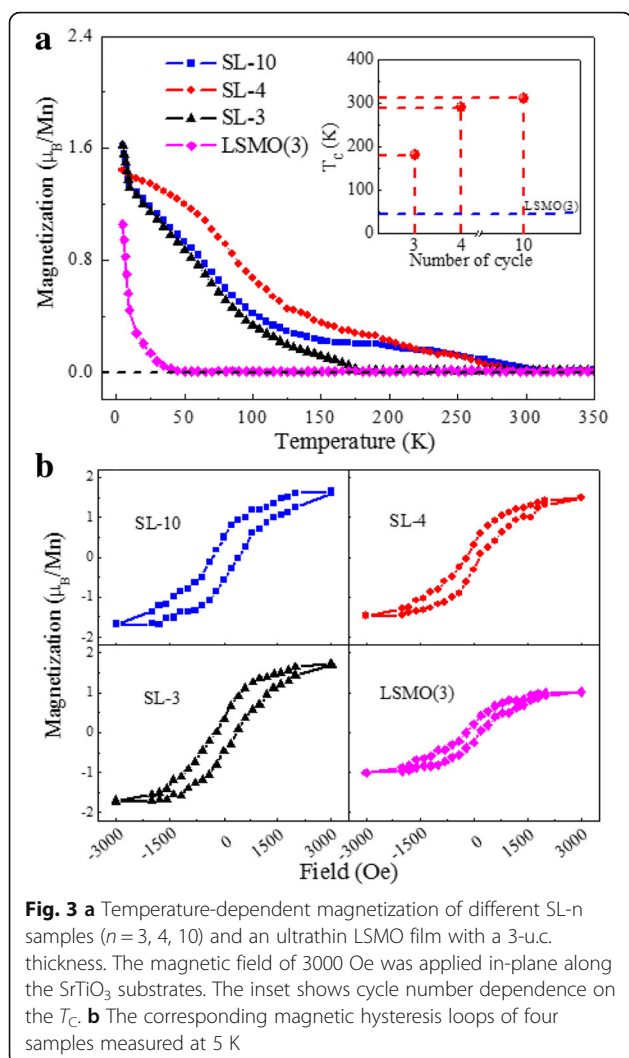


Fig. 3 **a** Temperature-dependent magnetization of different SL- n samples ($n = 3, 4, 10$) and an ultrathin LSMO film with a 3-u.c. thickness. The magnetic field of 3000 Oe was applied in-plane along the SrTiO_3 substrates. The inset shows cycle number dependence on the T_C . **b** The corresponding magnetic hysteresis loops of four samples measured at 5 K

LSMO layers, the M_s value of our SL- n films calculated from the original measurement data will become $\sim 4.5 \mu_B/\text{Mn}$, which will exceed the theoretical low temperature value of the LSMO ($\sim 3.67 \mu_B/\text{Mn}$) [34]. Note that the M_s per spin is much less than of bulk LSMO, suggesting either a fraction of nonmagnetic spins, a ferrimagnetic spin arrangement, or strong spin-canting [18, 35]. More work will be needed to quantify decreased M_s in this LSMO/BTO system. Also, the magnetic anisotropy of the SL- n samples with $n = 3, 4, 10$ were studied. The magnetic hysteresis loops for the magnetic field applied in-plane and out-of-plane measured at 5 K (not shown here) display that the easy magnetization axis for the three samples is parallel to the film plane direction, which is related to the orbital occupancy in LSMO layers, as discussed below.

We now focus on the correlation between increased T_C and electron orbital occupancy in the LSMO/BTO superlattices. It is known that the Mn^{3+} ions are Jahn-Teller active, and a slightly distorted orthorhombic

structure can stabilize one of the e_g orbitals. Supposing the $e_g(3z^2-r^2)$ is occupied, an interlayer double exchange interaction between the Mn^{3+} and Mn^{4+} ions will take place primarily along the c direction for (001)-oriented LSMO material. When $e_g(x^2-y^2)$ is occupied, the intra-layer double exchange will become very strong and the interlayer double exchange will decline in strength. In ultrathin films, in-plane interactions dominate the magnetic exchange and T_C . Thus, control of the orbital ordering is important for obtaining high-temperature ferromagnetism. That is to say, a high-occupancy probability of the $e_g(x^2-y^2)$ orbital can result in a high T_C for (001)-oriented LSMO films.

In our LSMO/BTO samples, the lattice parameter of the BTO ($a = 0.397\text{--}0.403$ nm from a tetragonal to rhombohedral phase) is larger than that of LSMO ($a = 0.387$ nm), resulting in a $\sim 4\%$ lattice mismatch [36–38]. Thus, the LSMO layers in our superlattices are in a high-tensile strain state ($c < a$), causing occupancy in the $e_g(x^2-y^2)$ orbital [39]. We now discuss the manganese e_g orbital occupancy in relation to XLD measurements, which is an extremely sensitive probe for the electronic structure and the d orbital (e_g) electron occupancy (schematic diagram shown in Fig. 4d), which has proven in referential occupancy at interfaces [14]. The XAS spectra were measured at the Mn $L_{2,3}$ -edges for the photon polarization (E) parallel to the sample plane (E_{\parallel}) and perpendicular to it (E_{\perp}). The XLD is calculated as the XAS intensity difference between the E_{\parallel} and E_{\perp} components to determine the occupancy of the Mn^{3+} e_g orbitals. In (001)-oriented LSMO films, the out-of-plane direction corresponds to [001], and the in-plane direction was obtained with $E_{\parallel}||[100]$, as shown in Fig. 4d. The area under the XLD curve at the L_2 -edge peak (ΔXLD) represents the difference between the relative occupancies of the $e_g(x^2 - y^2/3z^2 - r^2)$ orbitals. A positive/negative ΔXLD (on average) is ascribed attributed to a preferential occupancy of the $e_g(3z^2 - r^2)/(x^2 - y^2)$ orbitals for (001) LSMO films. Figure 4a, b shows the XLD spectra, as well as the in-plane and out-of-plane XAS spectra, of SL-3 and SL-10 samples. The ΔXLD area at the L_2 -edge peak is negative, implying a preferential occupancy of the $e_g(x^2-y^2)$ orbital (see Fig. 4e), which is consistent with the results reported by D. Pesquera et al. [39]. Consequently, in our LSMO/BTO superlattices, the interfacial tensile strain is originated from the lattice mismatch between the BTO and LSMO layers. It induces in-plane orbital ordering of the $e_g(x^2-y^2)$ orbital occupancy in the LSMO layers, achieving high T_C . This negative value of the ΔXLD area is also evidence that the Mn^{3+} ions in the LSMO triple layers have the same orbital occupancy, which contributes to high-temperature ferromagnetism. Also, the absolute value of ΔXLD for the SL-10 sample is

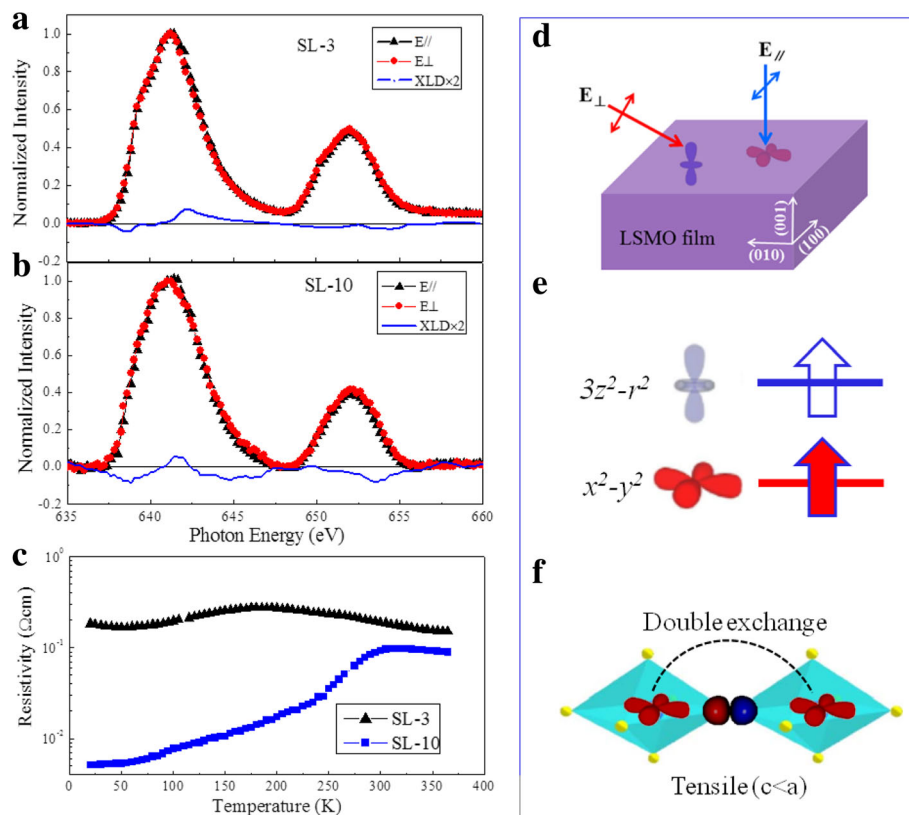


Fig. 4 **a, b** Normalized XAS and XLD curves for samples SL-3 and SL-10 measured at room temperature. **c** Temperature-dependent resistivity measured in the temperature range from 20 to 365 K for (001)-oriented SL-*n* samples where *n* = 3 and 10. **d** Experimental configuration diagram for XAS measurements with different X-ray incident angles. **e** Schematic representation of the electronic orbital occupancy of manganese e_g in (001)-oriented LSMO/BTO superlattices. **f** Proposed double exchange coupling mechanism along the in-plane direction

significantly larger than that of the SL-3 sample, which corresponds to the increased T_C seen in Fig. 3a.

Figure 4c shows temperature-dependent resistivity in the temperature range from 20 to 365 K for (001)-oriented SL-*n* superlattices with *n* = 3 and 10, respectively. The two samples exhibit a metal-to-insulator transition temperature (T_{MI}). The T_{MI} values of 178 and 310 K for samples SL-3 and SL-10, respectively, correspond to the T_C shown in Fig. 3a. This supports the scenario for a transition at T_C from a paramagnetic insulating phase to a ferromagnetic metallic phase. Thus, the high-temperature ferromagnetism originates from in-plane double exchange interactions between the Mn³⁺ and Mn⁴⁺ ions as shown in Fig. 4f [40, 41]. In-plane overlap between (partly filled) Mn e_g(x^2-y^2) with O 2 p_x and O 2 p_y creates stronger ferromagnetic coupling than that between (more empty) Mn e_g($3z^2-r^2$).

Conclusions

In summary, LSMO/BTO superlattices were prepared using PLD and the relationship between high T_C and manganese e_g orbital occupancy was revealed combined with XLD spectra. We showed that the regular

intercalation of BTO layers between LSMO layers effectively enhances ferromagnetic order and increases the T_C of LSMO/BTO superlattices. The preferential orbital occupancy of e_g(x^2-y^2) in LSMO layers induced by tensile strain of BTO layers is beneficial to the in-plane double exchange ferromagnetic coupling between Mn³⁺ and Mn⁴⁺ ions, resulting in a large T_C . Our findings create new opportunities for the design and control of magnetism in artificial structures and offer considerable potential for applications in novel magnetoelectronic applications, including nonvolatile magnetic memory working far above room temperature.

Abbreviations

AFM: Atomic force microscopy; BHF: NH₄F-buffered HF solution; FFT: Fast Fourier transform; M_s : Saturation magnetization; PLD: Pulsed laser deposition; PPMS: Physical properties measurement system; RHEED: Real-time reflection high-energy electron diffraction; SQUID: Superconducting quantum interference device; T_C : Curie temperature; TEM: Transmission electron microscopy; TEY: Total electron yield; T_{MI} : Metal-to-insulator transition temperature; XAS: X-ray absorption spectroscopy; XLD: X-ray linear dichroism; XRD: X-ray diffraction

Acknowledgements

The work is financially supported by the NSFC (nos. 51571136, 61434002, and 61306109), the Ministry of Education of China (no. IRT 1156), and Shanxi

Scholarship Council of China (no. 2015-069). The authors also acknowledge Beamline BL08U1A (Shanghai Synchrotron Radiation Facility, China) and U19 (National Synchrotron Radiation Laboratory, China) stations for XAS measurements.

Authors' Contributions

FZ, BW, and GZ performed the experiment and performed the tests on the samples. Z-YQ designed and performed the experiment, analyzed the results, and drafted the manuscript. X-HX supervised the work and revised the manuscript. All authors read and approved the final manuscript.

Competing Interests

The authors declare that they have no competing interests.

Publisher's Note

Springer Nature remains neutral with regard to jurisdictional claims in published maps and institutional affiliations.

Author details

¹Key Laboratory of Magnetic Molecules and Magnetic Information Materials of Ministry of Education, School of Chemistry and Materials Science, Shanxi Normal University, Linfen 041004, China. ²Research Institute of Materials Science, Shanxi Normal University, Linfen 041004, China. ³Suzhou Institute of Nano-Tech and Nano-Bionics, China Academy of Sciences, Suzhou 215123, China.

Received: 23 November 2017 Accepted: 9 January 2018

Published online: 17 January 2018

References

- Thiel S, Hammerl G, Schmehl A, Schneider CW, Mannhart J (2006) Tunable quasi-two-dimensional electron gases in oxide heterostructures. *Science* 313:1942–1945
- Hueso LE, Pruneda JM, Ferrari V, Burnell G, Valdes-Herrera JP, Simons BD, Littlewood PB, Artacho E, Fert A, Mathur ND (2007) Transformation of spin information into large electrical signals using carbon nanotubes. *Nature* 445:410–413
- Qin Q, He S, Song W, Yang P, Wu Q, Feng YP, Chen J (2017) Ultra-low magnetic damping of perovskite $\text{La}_{0.7}\text{Sr}_{0.3}\text{MnO}_3$ thin films. *Appl Phys Lett* 110:112401
- Liang L, Li L, Wu H, Zhu X (2014) Research progress on electronic phase separation in low-dimensional perovskite manganite nanostructures. *Nanoscale Res Lett* 9:325
- Zheng D, Jin C, Li P, Wang L, Feng L, Mi W, Bai H (2016) Orbital reconstruction enhanced exchange bias in $\text{La}_{0.6}\text{Sr}_{0.4}\text{MnO}_3$ /orthorhombic YMnO_3 heterostructures. *Sci Rep* 6:24568
- Huijben M, Martin LW, Chu YH, Holcomb MB, Yu P, Rijnders G, Blank DHA, Ramesh R (2008) Critical thickness and orbital ordering in ultrathin $\text{La}_{0.7}\text{Sr}_{0.3}\text{MnO}_3$ films. *Phys Rev B* 78:094413
- Yamada M, Ogawa Y, Sato YH, Kawasaki M, Akoh H, Tokura Y (2004) Engineered interface of magnetic oxides. *Science* 305:646–648
- Peng R, Xu HC, Xia M, Zhao JF, Xie X, Xu DF, Xie BP, Feng DL (2014) Tuning the dead-layer behavior of $\text{La}_{0.67}\text{Sr}_{0.33}\text{MnO}_3/\text{SrTiO}_3$ via interfacial engineering. *Appl Phys Lett* 104:081606
- Infante IC, Sánchez F, Fontcuberta J, Wojcik M, Jedryka E, Estradé S, Peiró F, Arbiol J, Llokhin V, Espinós JP (2007) Elastic and orbital effects on thickness-dependent properties of manganite thin films. *Phys Rev B* 76:224415
- Mundy JA, Hikita Y, Hidaka T, Yajima T, Higuchi T, Hwang HY, Muller DA, Kourkoutis LF (2014) Visualizing the interfacial evolution from charge compensation to metallic screening across the manganite metal–insulator transition. *Nat Commun* 5:3464
- Xie C, Budnick JI, Wells BO, Woicik JC (2007) Separation of the strain and finite size effect on the ferromagnetic properties of $\text{La}_{0.5}\text{Sr}_{0.5}\text{CoO}_3$ thin films. *Appl Phys Lett* 91:172509
- Ziese M, Semmelhack HC, Han KH (2003) Strain-induced orbital ordering in thin $\text{La}_{0.7}\text{Ca}_{0.3}\text{MnO}_3$ films on SrTiO_3 . *Phys Rev B* 68:134444
- Tebano A, Aruta C, Sanna S, Medaglia PG, Balestrino G, Sidorenko AA, De Renzi R, Ghiringhelli G, Braicovich L, Bisogni V, Brookes NB (2008) Evidence of orbital reconstruction at interfaces in ultrathin $\text{La}_{0.67}\text{Sr}_{0.33}\text{MnO}_3$ films. *Phys Rev Lett* 100:137401
- Tebano A, Orsini A, Medaglia PG, Castro DD, Balestrino G, Freelon B, Bostwick A, Chang YJ, Gaines G, Rotenberg E, Saini NL (2010) Preferential occupation of interface bands in $\text{La}_{2/3}\text{Sr}_{1/3}\text{MnO}_3$ films as seen via angle-resolved photoemission. *Phys Rev B* 82:214407
- Ma JX, Liu XF, Lin T, Gao GY, Zhang JP, Wu WB, Li XG, Shi J (2009) Interface ferromagnetism in (110)-oriented $\text{La}_{0.7}\text{Sr}_{0.3}\text{MnO}_3/\text{SrTiO}_3$ ultrathin superlattices. *Phys Rev B* 79:174424
- Choi E-M, Kleibecker JE, Fix T, Xiong J, Kinane CJ, Arena D, Langridge S, Chen A, Bi Z, Lee JH, Wang H, Jia Q, Blamire MG, MacManus-Driscoll JL (2016) Interface-coupled $\text{BiFeO}_3/\text{BiMnO}_3$ superlattices with magnetic transition temperature up to 410 K. *Adv Mater Interfaces* 3:1500597
- Choi EM, Kleibecker JE, JL MM-D (2017) Strain-tuned enhancement of ferromagnetic T_C to 176 K in Sm-doped BiMnO_3 thin films and determination of magnetic phase diagram. *Sci Rep* 7:43799
- Boschker H, Kautz J, Houwman EP, Siemons W, Blank DHA, Huijben M, Koster G, Vaillonis A, Rijnders G (2012) High-temperature magnetic insulating phase in ultrathin $\text{La}_{0.67}\text{Sr}_{0.33}\text{MnO}_3$ films. *Phys Rev Lett* 109:157207
- Bowen M, Bibes M, Barthelemy A, Contour JP, Anane A, Lemaître Y, Fert A (2003) Nearly total spin polarization in $\text{La}_{2/3}\text{Sr}_{1/3}\text{MnO}_3$ from tunneling experiments. *Appl Phys Lett* 82:233–235
- Zhou G, Guan X, Bai Y, Quan Z, Jiang F, Xu X (2017) Interfacial spin glass state and exchange bias in the epitaxial $\text{La}_{0.7}\text{Sr}_{0.3}\text{MnO}_3/\text{LaNiO}_3$ bilayer. *Nanoscale Res Lett* 12:330
- Park JH, Vescovo E, Kim HJ, Kwon C, Ramesh R, Venkatesan T (1998) Direct evidence for a half-metallic ferromagnet. *Nature* 392:794–796
- Quan Z, Wu B, Zhang F, Zhou G, Zang J, Xu X (2017) Room temperature insulating ferromagnetism induced by charge transfer in ultrathin (110) $\text{La}_{0.7}\text{Sr}_{0.3}\text{MnO}_3$ films. *Appl Phys Lett* 110:072405
- Štrbik V, Reiffers M, Dobročka E, Šoltýs J, Španková M, Chromík Š (2014) Epitaxial LSMO thin films with correlation of electrical and magnetic properties above 400K. *Appl Surf Sci* 312:212–215
- Yin L, Zhang Q, Li D, Mi WB, Wang X (2016) Electric field modulation on special interfacial magnetic states in tetragonal $\text{La}_{2/3}\text{Sr}_{1/3}\text{MnO}_3/\text{BiFeO}_3$ heterostructures. *J Phys Chem C* 120:15342–15348
- Werner R, Petrov AY, Mno LA, Kleiner R, Koelle D, Davidson BA (2011) Improved tunneling magnetoresistance at low temperature in manganite junctions grown by molecular beam epitaxy. *Appl Phys Lett* 98:162505
- Feng N, Mi WB, Wang X, Cheng Y, Schwingenschlögl U (2015) Superior properties of energetically stable $\text{La}_{2/3}\text{Sr}_{1/3}\text{MnO}_3$ /tetragonal BiFeO_3 multiferroic superlattices. *ACS Appl Mater Interfaces* 7:10612–10616
- Matou T, Takeshima K, Anh LD, Seki M, Tabata H, Tanaka M, Ohya S (2017) Reduction of the magnetic dead layer and observation of tunneling magnetoresistance in $\text{La}_{0.67}\text{Sr}_{0.33}\text{MnO}_3$ -based heterostructures with a LaMnO_3 layer. *Appl Phys Lett* 110:212406
- Yin L, Zhang Q, Mi WB, Wang X (2016) Strain-controlled interfacial magnetization and orbital splitting in $\text{La}_{2/3}\text{Sr}_{1/3}\text{MnO}_3$ /tetragonal BiFeO_3 heterostructures. *J Appl Phys* 120:165303
- Ziese M, Bern F, Pippel E, Hesse D, Vrejoiu I (2012) Stabilization of ferromagnetic order in $\text{La}_{0.7}\text{Sr}_{0.3}\text{MnO}_3$ - SrRuO_3 superlattices. *Nano Lett* 12:4276–4281
- Sadoc A, Mercey B, Simon C, Grebille D, Prellier W, Lepetit MB (2010) Large increase of the Curie temperature by orbital ordering control. *Phys Rev Lett* 104:046804
- Kreisel J, Lucazeau G, Dubourdieu C, Rosina M, Weiss F (2002) Raman scattering study of $\text{La}_{0.7}\text{Sr}_{0.3}\text{MnO}_3/\text{SrTiO}_3$ multilayers. *J Phys Condens Matter* 14:5201
- Bormann D, Desfeux R, Degave F, Khelifa B, Hamet JF, Wolfman J (1999) Lattice mismatch effects between the substrate and GMR $\text{La}_{0.7}\text{Sr}_{0.3}\text{MnO}_3$ thin films studied by scanning probe microscopy and Raman spectroscopy. *Phys Stat Sol (b)* 215:691–695
- Martincarron L, Andres AD, Martinezlope MJ, Casais MT, Alonso JA (2002) Raman phonons as a probe of disorder, fluctuations and local structure in doped and undoped orthorhombic and rhombohedral manganites. *Phys Rev B* 66:174303
- Böttcher D, Henk J (2013) Magnetic properties of strained $\text{La}_{2/3}\text{Sr}_{1/3}\text{MnO}_3$ perovskites from first principles. *J Phys Condens Matter* 25:136005
- Mizumaki M, Chen WT, Saito T, Yamada I, Attfield JP, Shimakawa Y (2011) Direct observation of the ferrimagnetic coupling of A-site Cu and B-site Fe spins in charge-disproportionated $\text{CaCu}_3\text{Fe}_2\text{O}_{12}$. *Phys Rev B* 84:094418
- Murugavel P, Prellier W (2006) The magnetotransport properties of $\text{La}_{0.7}\text{Sr}_{0.3}\text{MnO}_3/\text{BaTiO}_3$ superlattices grown by pulsed laser deposition technique. *J Appl Phys* 100:023520

37. Chang K-S, Aronova MA, Lin C-L, Murakami M, Yu M-H, Hatrick-Simpers J, Famodu OO, Lee SY, Ramesh R, Wuttig M, Takeuchi I, Gao C, Bendersky LA (2004) Exploration of artificial multiferroic thin-film heterostructures using composition spreads. *Appl Phys Lett* 84:30913093
38. Xiao CJ, Jin CQ, Wang XH (2008) Crystal structure of dense nanocrystalline BaTiO₃ ceramics. *Mater Chem Phys* 111:209–212
39. Pesquera D, Herranz G, Barla A, Pellegrin E, Bondino F, Magnano E, Sanchez F, Fontcuberta J (2012) Surface symmetry-breaking and strain effects on orbital occupancy in transition metal perovskite epitaxial films. *Nat Commun* 3:1189
40. Zener C (1951) Interaction between the d-shells in the transition metals. II. Ferromagnetic compounds of manganese with perovskite structure. *Phys Rev* 82:403
41. de Gennes PG (1960) Effects of double exchange in magnetic crystals. *Phys Rev* 118:141

Submit your manuscript to a SpringerOpen[®] journal and benefit from:

- Convenient online submission
- Rigorous peer review
- Open access: articles freely available online
- High visibility within the field
- Retaining the copyright to your article

Submit your next manuscript at ► [springeropen.com](https://www.springeropen.com)